

All-optical bandwidth-tailorable radar

Weiwen Zou^{1,2}, Hao Zhang¹, Xin Long¹, Siteng Zhang¹, Yuanjun Cui¹, and Jianping Chen^{1,2}

¹*State Key Laboratory of Advanced Optical Communication Systems and Networks, Department of Electronic Engineering, Shanghai Jiao Tong University, Shanghai 200240, China*

²*Shanghai Key Lab of Navigation and Location Services, Shanghai Jiao Tong University, Shanghai 200240, China*

ABSTRACT

Radar has been widely used in military, security, and rescue. Metamaterial cloak is employed in stealth targets to evade radar detection. Hence modern radar should be reconfigurable at multi-bands for detecting stealth targets, which might be realized based on microwave photonics. Here, we demonstrate an all-optical bandwidth-tailorable radar architecture. It is a coherent system utilizing one mode-locked laser for both signal generation and reception. Heterodyning of two individually filtered optical pulses that are pre-chirped via wavelength-to-time mapping generates wideband linearly-chirped radar signal. The working bands can be flexibly tailored with desired bandwidth at user-preferred carrier frequency. After modulated onto the pre-chirped optical pulse, radar echoes are time-stretched and frequency-compressed by several times. The digitization becomes much easier without loss of detection ability. We believe that the demonstration can innovate the radar's architecture with ultra-high range resolution.

Introduction

Like any other wireless equipment, conventional microwave and millimeter-wave radar system can only work well on a pre-designed band and inevitably requires up-conversion and down-conversion procedures ¹⁻⁴. Radar waveforms at baseband are synthesized by digital electronics and then up-converted to the carrier frequency. In reception, radar echoes need to be electronically down-converted before signal processing. Metamaterials with distinctive electromagnetic scattering characteristics ⁵⁻⁷ were proposed to evade radar detection by covering a target with a metamaterial cloak. Electromagnetic waves are absorbed or scattered by the cloak, hence the radar cross-section is effectively reduced and the target cannot be perceived. However, such a kind of cloak is hardly perfect since it can only work at a particular frequency band. In order to improve performance in detecting stealth target, modern radar should be reconfigurable and capable of working at multi-bands. Because frequency characteristics of microwave components are usually fixed, a radar system capable of working at multi-bands should have an array of generating/transmitting and receiving/processing units which is composed of several sets of frequency conversion components, thus making the system very complicated. Linearly-chirped waveform is one of the most commonly used radar signals and extensively employed in modern radar system to improve range resolution, dynamic range, and/or signal-to-noise ratio based on pulse compression technology ¹⁻². Photonics-assisted radio-frequency (RF) technology, nominated microwave photonics ⁸⁻⁹, can provide better flexibility for signal generation of linearly-chirped waveform ¹⁰⁻²² so as to overcome the limits of bandwidth and time jitter of the modern electronic or microwave devices. Therefore, microwave photonics has been considered as a key technology for future radars ²³⁻²⁴.

In this article, we propose an all-optical bandwidth-tailorable radar architecture.

Linearly-chirped signals are optically generated or received without any assistance of

electronic up-conversion and down-conversion procedures so that this architecture is in principle more advanced and more reconfigurable than ²³. When detecting a stealth target, it is capable to rapidly tailor among different operating bands by simply adjusting the optical devices. Since the current cloak technique cannot ensure full bandwidth covering, the radar cross-section might be large at certain bands, which greatly increases the possibility to successfully detect the cloaked target via this architecture. In reception, the received radar echoes are optically stretched in time domain and compressed in frequency domain, which is equivalently down-converted. Hence, electronic down-conversion is avoided and analog-to-digital conversion (ADC) sampling rate is essentially reduced.

Results

Principle and experimental setup. Figure 1 shows the setup and principle of the proposed all-optical bandwidth-tailorable radar. Only one mode-locked laser (MLL) is used as the optical source for both signal generation and reception, ensuring the strict coherence of the whole system. In signal generation part, one dispersion element (DE1) with relatively large dispersion value is laid after the MLL. Due to the wide optical spectrum of the MLL, the short optical pulse train is broadened or chirped in time domain with the same repetition rate. The time profile is the same as the optical spectrum because of the linear dispersion used. An optical coupler (OC1) divides the chirped optical signal into two parts for signal generation and reception, respectively. Another optical coupler (OC2) divides the optical pulse train into two arms for signal generation. Two tunable optical filters (TOFs) with approximately rectangular filtering characteristics are placed in two arms to tailor certain parts of the optical spectra. According to the Fourier transformation or wavelength-to-time mapping introduced by dispersion, filtered wideband optical spectra are linearly mapped to time domain. Therefore, the temporal and spectral profiles of the filtered pulses in two arms are

almost rectangular. A second dispersion element (DE2) with a small dispersion value is added in the first arm to induce dispersion difference between two arms so that the temporal duration of the pulse in the first arm becomes wider (or narrower) than that in the second arm according to the dispersion sign of DE2. In order to compensate for the time difference between pulses in two arms, a variable optical delay line (VODL1) is inserted in the second arm. After heterodyning, that is, beating of two differently dispersed optical pulses at the optical coupler (OC3) and opto-electronic conversion at a high-speed photo-detector (PD1), the generated RF signal is linearly-chirped in frequency. The carrier frequency and sweep bandwidth are determined by the difference of central wavelengths and filtering bandwidth of TOFs, respectively. This approach without any electronic devices can be used to easily tailor different carrier frequency and sweep bandwidth by simply tuning the two TOFs, which is schematically shown in the inset (i) of Fig. 1.

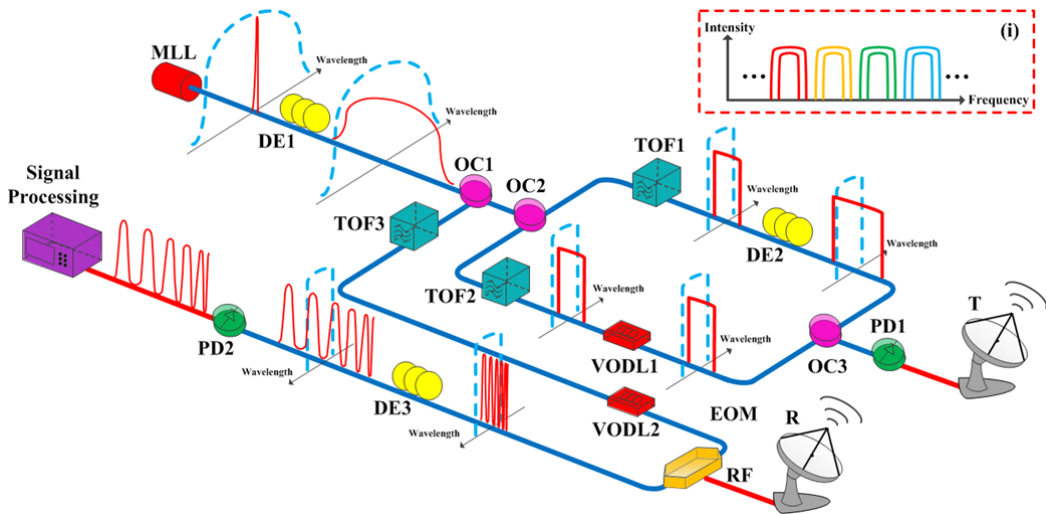


Figure 1: Architecture of all-optical bandwidth-tailorable radar. A MLL with broadband optical spectra is used as the optical source for both signal generation and reception. DE1 maps the broad optical spectra of short pulse train to the time domain. After coupled into two arms and filtered by two TOFs, signal in each arm becomes an approximately rectangular profile. The signal in the first arm is temporally stretched wider than that in the second arm since DE2 is added. The detected linearly-chirped signal is emitted by the transmitting (T) antenna. The echo pulses received by the receiving (R) antenna are directed to the RF port of EOM. TOF3 filters the pre-chirped optical pulse train from OC1. VODL2 compensates for time difference between the optical and electrical signals into EOM. DE3 further stretches the modulated optical signal. After opto-electronic conversion, the received echoes are temporally stretched. Signal processing module digitalizes the time-stretched signal. The inset denotes how different carrier frequency and/or different sweep bandwidth is generated.

In the reception part, frequency of the echoes is tailored and bandwidth is compressed based on the time-stretch principle. Up to date, the time-stretch principle has been widely used in photonic ADC, rogue measurement, biomedical imaging, and hardware accelerator²⁵⁻³³. As shown in Fig. 1, received radar echoes are directed to the RF port of an electro-optic modulator (EOM). They are modulated onto the pre-chirped and filtered optical carrier divided from OC1. The filtering bandwidth of TOF3 is set wider than TOF1 and TOF2 since the temporal duration of radar echoes for multi-target detection is usually longer. Wider filtering bandwidth ensures that the echoes can be modulated onto the optical carrier. Another variable optical delay line (VODL2) is inserted between the TOF3 and EOM to compensate for the time difference between the optical carrier and the radar echoes to be modulated. A third dispersion element (DE3) with larger dispersion value than DE1 is placed after EOM to further enlarge the modulated optical pulses. When detected by a lower-speed photo-detector (PD2), the signals are time-stretched and frequency-compressed by several times compared with the original radar echoes. Therefore, the ADC sampling rate after the reception part can be lowered correspondingly.

All-optical radar signal generation. As a proof of concept, wideband linearly-chirped signal with great time-bandwidth product (TBWP) and signals at three tailored frequency bands are demonstrated. Figure 2 shows the measurement results of the generated signals. Constrained by current testing condition, we have only demonstrated signal under the bandwidth limit (~63 GHz) of the oscilloscope. Figure 2a-d demonstrates the results when the waveform is designed to cover a rather wide bandwidth with a repetition rate of 37 MHz (i.e. 27-ns period) as the used MLL. The duration of each pulse lasts ~23 ns and the short time Fourier transform (STFT) analysis shows that the generated signal covers a bandwidth from 5 GHz to 60 GHz, resulting in a large TBWP of ~1265. It is the largest TBWP record to the best of our knowledge for methods based on the wavelength-to-time mapping principle. We also calculated the

autocorrelation of each pulse to evaluate the pulse compression capability of the generated signal. Owing to the wide bandwidth, the pulse duration is compressed to ~ 9 ps with the period of ~ 27 ns. Figure 2e-g denotes the STFT analysis of the tailored signals in X-band, Ku-band, and Ka-band, respectively. The carrier frequency and bandwidth are independently tunable by adjusting the central wavelength and filtering bandwidth of two TOFs. Waveforms in the three bands maintain the same chirp rate since it is in principle determined by the dispersion values of DE1 and DE2. In the demonstrated results, the 37 MHz pulse envelope has been eliminated and detailed processing method can be referred to the **Methods**.

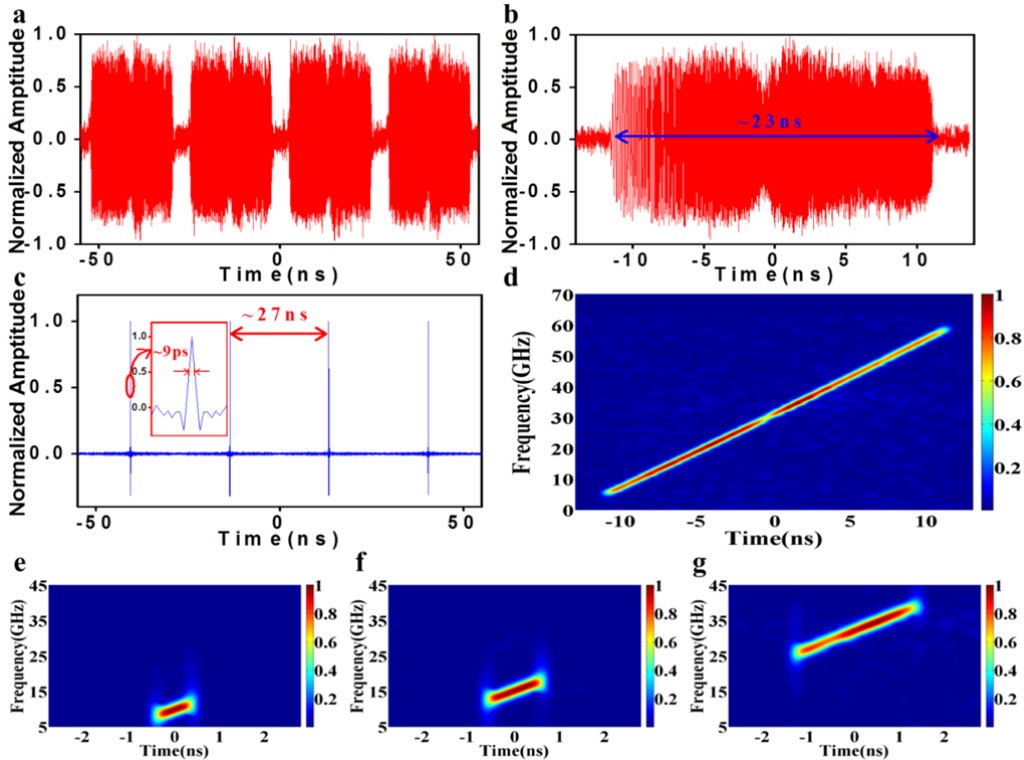


Figure 2: Measurement results of the generated signals. **a**, Generated linearly-chirped pulse train covering an ultra-broad wideband from 5 GHz to 60 GHz with a repetition rate of 37 MHz and a large TBWP of ~ 1265 . **b**, The magnified temporal waveform of the generated signal in **a**. **c**, The autocorrelation of the generated linearly-chirped pulse train in **a**. The temporal width of the compressed pulse shows the pulse compression capability of the generated signal when used for detection. **d**, The short time Fourier transform (STFT) analysis of the generated signal in **a**. **e**, The STFT analysis of the generated X-band signal. **f**, The STFT analysis of the generated Ku-band signal. **g**, The STFT analysis of the generated Ka-band signal.

All-optical radar signal reception. Single-target detection experiment was conducted to verify the proposed bandwidth-tailorable reception. As illustrated in Fig. 3a, frequency components are compressed and temporal durations are expanded in the signal reception part. Suppose DE1 and DE3 are the same kind of optical fibres and L_1 and L_3 are their individual lengths. Then, the frequency components are tailored or compressed by the factor of M ($=L_3/L_1+1$), called the time-stretch ratio²⁵, since the temporal duration of the echoes is expanded by M times with respect to the original duration t_0 . If M is large enough, the high frequency signal can be converted to the low frequency signal. The X-band linearly-chirped signal described in Fig. 2e is employed as an example. Figure 3b-c illustrate the schematic diagram and experimental layout, respectively. The all-optically generated X-band signal is amplified by a power amplifier (PA) and transmitted by a horn antenna. The received echo collected by another horn antenna is firstly amplified by a low noise amplifier (LNA) and goes through the signal reception part. The two horn antennas are positioned approximately side by side. A metal plate is placed in front of the antennas as the reflective target. A comparison of signals before transmission and after time-stretched reception is given in Fig. 3d-g. The waveform in Fig. 3d lasts ~ 1 ns while that in Fig. 3e lasts ~ 5 ns, indicating $M = \sim 5$. Figure 3f-g are their STFT analysis results, respectively. Compared with the original transmitted signal, the time-stretched echo has been compressed by ~ 5 times. The central frequency of the signal after reception locates at ~ 2 GHz and the linearly-chirped feature has been retained. This demonstration proves the ability of signal reception part to equivalently down-convert echoes and alleviate the demand of sampling rate.

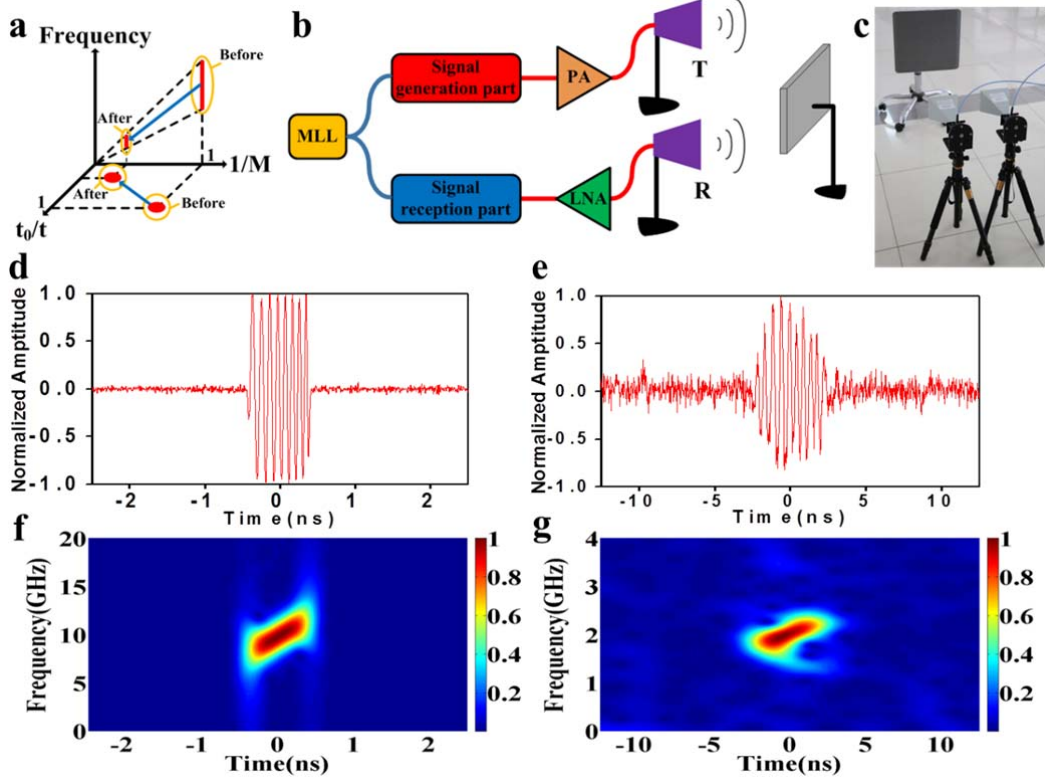


Figure 3: Principle and measurement results for time-stretched reception. **a**, Principle of time-stretched reception. **b**, Schematic diagram of single-target detection. **c**, Experimental layout of single-target detection. **d**, Temporal waveform of the transmitted X-band signal. **e**, Temporal waveform of the received X-band echo after time-stretched process. The stretch ratio is $M = \sim 5$. **f**, The STFT analysis of the transmitted X-band signal. **g**, The STFT analysis of the received X-band signal after time-stretched process. The stretch ratio is $M = \sim 5$.

Radar detection ability. Range resolution is usually used to characterize the detection ability. In order to better distinguish two or more neighbouring targets, linearly-chirped waveform with broader bandwidth is desired. The generated X-band signal is used again as an example to perform a dual-target detection. The schematic diagram and experimental layout are illustrated in Fig. 4a-b. Two metal plates are placed side by side but separated by a distance of ΔD along the ranging direction. Fig. 4c-d are the normalized echoes after the compressed reception when ΔD is changed. The horizontal axis is the round-trip time for travelling. The reflected echoes are obviously overlapped in the time domain in Fig. 4c when targets are very close, which might result in

ambiguity. When ΔD increases, the two reflected echoes split and become easy to be distinguished even without signal processing. After the matched filtering processing explained in the **Methods**, we obtain the results of the normalized cross-correlation power between the measured waveforms in Fig. 4c-d and the reference signal that is the time-stretched waveform achieved in the single-target detection (see Fig. 3e). As depicted in Fig. 4e-f, two reflection peaks can be clearly distinguished in the ranging result. The coordinate in the down horizontal axis are 5 times as that in the up horizontal axis. They respectively represent the distance calculated using the time axis of Fig. 4c-d and the real distance before time stretch. It is noted that the real distance corresponds to the radar's one-way transmitting distance from the targets to the transceiver or receiver antenna. The peak height is essentially influenced by the radar cross-section as well as the reflection angle of the metal plate. The left peak is roughly positioned at ~ 80 cm, while the right peak moves after ΔD is increased. The measured distance between these two peaks indicates that the distance between the targets is increased from ~ 6.3 cm to ~ 15.0 cm. The pulse widths at the half maximum (i.e. ~ 5.4 cm and ~ 5.7 cm) are approximately equal to each other, denoting the range resolution of the all-optical radar at the tailored X-band. It is maintained as the order of magnitude for the transmitted signal (centered at 10 GHz, 4 GHz bandwidth) but not determined by the time-stretched signal (centered at 2 GHz, 0.8 GHz bandwidth). Therefore, the detection ability is not lost after the time-stretched reception.

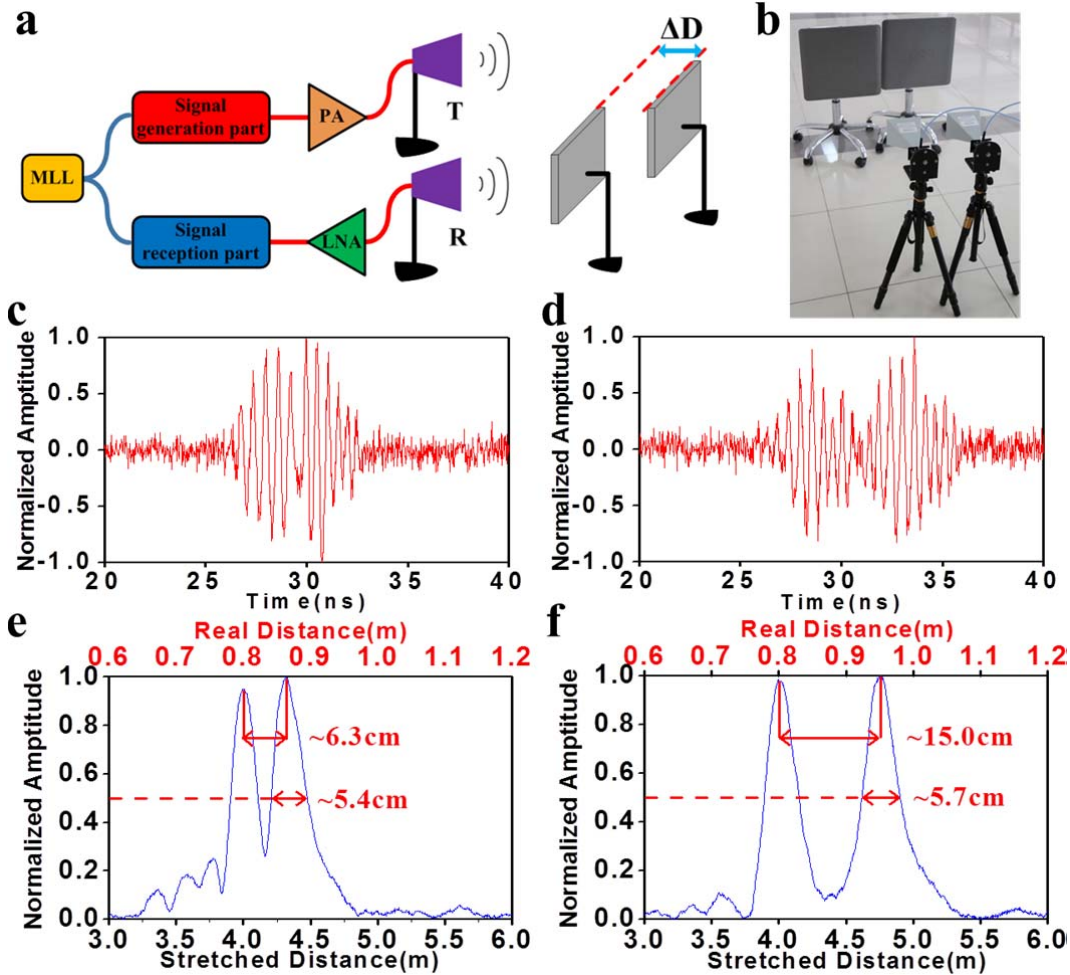


Figure 4: Measurement results of the dual-target detection. **a**, Schematic diagram of dual-target detection. **b**, Experimental layout of dual-target detection. **c**, The received echo when the distance between dual targets is ~ 6.3 cm. **d**, The received echo when the distance between dual targets is ~ 15.0 cm. **e**, Result after matched filtering processing when the distance between dual targets is ~ 6.3 cm. **f**, Result after matched filtering processing when the distance between dual targets is ~ 15.0 cm.

Discussions

The proposed all-optical bandwidth-tailorable radar architecture is strictly coherent since both signal generation and reception originate from the same MLL as the optical source. Owing to the seamless convergence of the wavelength-to-time mapping and time-stretch principle, high-resolution ranging with low sampling rate is ensured. The radar can be easily tailorable for different central frequencies and different sweep

bandwidths by simply adjusting the TOFs and its electromagnetic properties of the targets suffer no loss after the time-stretched processing. With an appropriate PD, frequency regions can be extended even higher to millimetre-waves²². Although the tailored X-band is illustrated as an example for dual-target detection and verification of the detection ability, it is no doubt that the effectiveness of the radar with broader bandwidth and better range resolution at higher-frequency bands is expectable if the RF front-end (power amplifiers and antennas) are correspondingly switched. Besides, two antennas for transmission and receptions are used in this work, while a bistatic antenna as utilized in²³ might works properly. The measurement range of the radar (~ 4 m) is limited by the period of the MLL (27 ns) used in this work. However, the measurement range might be extended by use of advanced radar signal processing¹⁻² or by substitution of a MLL with lower repetition rate.

Methods

Experimental components. We used a mode-locked fibre laser (Precision photonics Corp., FFL-1560-B) with the repetition rate of 37 MHz as the optical source. The oscilloscope (Agilent Technology Ltd. now called Keysight Technology Ltd., DSAX96204Q) with 63 GHz bandwidth was used to capture signals. Three tunable optical filters (Alnair Labs, CVF-220CL) were used in the experimental setup. Two of them were placed in two arms to pick out certain parts of the optical spectra for signal generation and the third one was used to generate the optical carrier for signal reception. In Fig. 2a-d, the dispersion value of DE1, filtering bandwidth of TOF1 and TOF2, central wavelength difference between TOF1 and TOF2 are ~ 3863 ps², ~ 8 nm, ~ 0.26 nm, respectively. A SMF of ~ 9 km was used as DE2. In Fig. 2e-g, the dispersion value of DE1 is ~ 380 ps² and ~ 200 -meter SMF was used as DE2. The filtering bandwidth of TOF1 and TOF2 are ~ 2.4 nm (X-band), ~ 3.6 nm (Ku-band), and ~ 8.4 nm (Ka-band).

The central wavelength difference between TOF1 and TOF2 are \sim 0.08 nm (X-band), \sim 0.12 nm (Ku-band), \sim 0.26 nm (Ka-band). In Fig. 3, the horn antennas (LB-90-20-C-SF) for signal transmitting and receiving were mounted on two tripods. The power amplifier (Multilink Technology Corporation, MTC5515) and low noise amplifier (TLA-060120G36) both have a relatively flat gain in 8-12 GHz. The dispersion value of DE3 for the time-stretched processing is \sim 1915 ps². The PD1 (Finisar, XPDV4120R) and PD2 (Discovery DSC720) are used, respectively. The metal plates used as targets have the size of 40 cm \times 40 cm.

Pulse-envelope elimination. As depicted in the temporal waveforms in Fig. 2, the linearly-chirped waveform does not have an envelope of pulses at the repetition rate of 37 MHz. That is because the measured data has been subtracted by the average waveform over thousands of times to cancel the envelope of pulses at 37 MHz. In Fig. 5a, the original linearly-chirped signal has an envelope of approximately rectangular profile. As can be seen in its short time Fourier transform (STFT) analysis in Fig. 5b, there exists strong low frequency components. The average waveform over thousands of times is shown in Fig. 5c, and the magnified STFT is depicted in Fig. 5d. Note that this low frequency components can be also eliminated by a high-bandwidth-pass electronic filter before the power amplifier. When processing the temporal waveforms in Fig. 3 and Fig. 4, we also use this numerical method to eliminate the pulse envelop.

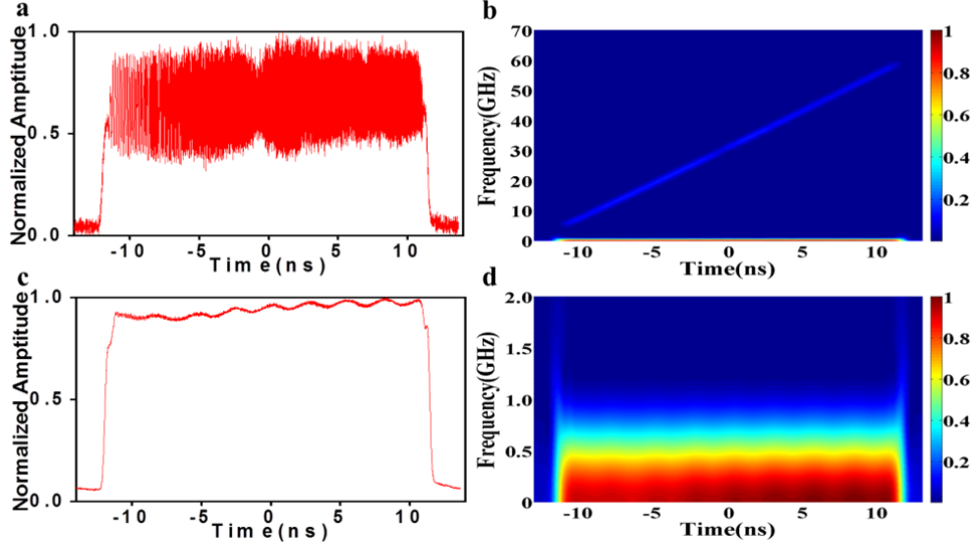


Figure 5: Example of pulse-envelope elimination. **a.** The original waveform of the linearly-chirped signal covering a wideband from 5 GHz to 60 GHz. **b.** The STFT analysis of the linearly-chirped signal in **a.** **c.** The average waveform of the linearly-chirped signal. **d.** The magnified view of the STFT analysis of the linearly-chirped signal in the low frequency range.

Matched filtering processing. The matched filtering process of the received echoes in Fig. 4 is calculated based on the following algebra:

$$y_{MF}(t) = x_{back}(t) \otimes x_{ref}^*(-t) \quad (1)$$

where $x_{back}(t)$ represents the time-stretched echoes and $x_{ref}^*(t)$ the conjugate of the time-reversed reference signal. Numerical implementation of the matched filtering process is described as follows:

- In order to perform the matched filtering processing, a reference waveform is needed. The reference waveform we used to calculate Fig. 4 is the waveform shown in Fig. 3e, which is the reflected echo acquired when a single target is placed in the beam path.
- Since the captured data using the oscilloscope only has real value. The measured waveforms in Fig. 4c-d and the reference waveform are respectively transformed to complex value through Hilbert transformation to fulfill I/Q demodulation.

- c) The complex echoes are cross-correlated with the complex reference signal to fulfill the matched filtering according to Eq. (1). Consequently, the linearly-chirped echoes are compressed to separate peaks.
- d) The obtained pulse compression results are plotted versus both time-stretched distance (the down horizontal axis) and the real distance before the time-stretched processing (the up horizontal axis).

References:

1. Skolnik, M. *Introduction to radar systems* (McGraw-Hill, 2001).
2. Richards, M., Scheer, J. & Holm, W. *Principles of modern radar: basic principles* (SciTech Pub., 2010).
3. Nag, S., Barnes, M., Payment, T. & Holladay, G. Ultrawideband through-wall radar for detecting the motion of people in real time. *Proc. SPIE, Radar Sensor Technology and Data Visualization* **4744**, 48-57 (2002).
4. Li, C., Lubecke, V., Boric-Lubecke, O. & Lin, J. A review on recent advances in Doppler radar sensors for noncontact healthcare monitoring. *IEEE Trans. Microwave Theory Tech.* **61**, 2046-2060 (2013)
5. Schurig, D., Mock, J., Justice, B. *et al.* Metamaterial electromagnetic cloak at microwave frequencies. *Science* **314**, 977-980 (2006).
6. Valentine, J., Zhang, S., Zentgraf, T. *et al.* Three-dimensional optical metamaterial with a negative refractive index. *Nature* **455**, 376-379 (2008).
7. Landy, N., Sajuyigbe, S. Mock, J. *et al.* Perfect metamaterial absorber. *Phys. Rev. Lett.* **100**, 207402 (2008)
8. Capmany, J. & Novak, D. Microwave photonics combines two worlds. *Nature Photon.* **1**, 319-330 (2007).
9. Yao, J. Microwave photonics. *J. Lightwave Technol.* **27**, 314-335 (2009).
10. Yao, J. Photonic generation of microwave arbitrary waveforms. *Opt. Commun.* **284**, 3723-3736 (2011).
11. Li, W. Kong, F. & Yao, J. Arbitrary microwave waveform generation based on a tunable optoelectronic oscillator. *J. Lightwave Technol.* **31**, 3780-3786 (2013).
12. Li, W. & Yao, J. Generation of linearly chirped microwave waveform with an increased time-bandwidth product based on a tunable optoelectronic oscillator and a recirculating phase modulation loop. *J. Lightwave Technol.* **32**, 3573-3579 (2014).
13. Chou, J., Han, Y. & Jalali, B. Adaptive RF-photonic arbitrary waveform generator. *IEEE Photonics Technol. Lett.* **15**, 581-583 (2003).
14. McKinney, J. D., Seo, D., Leaird, D.E. & Weiner A. M. Photonically assisted generation of arbitrary millimeter-wave and microwave electromagnetic waveforms via direct space-to-time optical pulse shaping. *J. Lightwave Technol.* **21**, 3020-3028 (2003).
15. Ashrafi, R., Park, Y. & Azana, J. Fiber-based photonic generation of high-frequency microwave pulses with reconfigurable linear chirp control. *IEEE Trans. Microwave Theory Tech.* **58**, 3312-3319 (2010).
16. Wong, J. H., Liu, H. H., Lam, H. Q., Aditya, S., Zhou, J., Lim, P. H., Lee, K. E. K., Wu, K., Chow K. K. & Shum, P. P. Photonic generation of microwave waveforms with wide chirp tuning range. *Opt. Commun.* **304**, 102-106 (2013).
17. Li, M. & Yao, J. Photonic generation of continuously tunable chirped microwave waveforms based on a temporal interferometer incorporating an optically pumped linearly chirped fiber Bragg grating. *IEEE Trans. Microwave Theory Tech.* **59**, 3531-3537 (2011).
18. Zeitouny, A., Stepanov, S., Levinson, O. & Horowitz, M. Optical generation of linearly chirped microwave pulses using fiber Bragg gratings. *IEEE Photonics Technol. Lett.* **17**, 660-662 (2005).

19. Wang, C. & Yao, J. Chirped microwave pulse generation based on optical spectral shaping and wavelength-to-time mapping using a Sagnac loop mirror incorporating a chirped fiber Bragg grating. *J. Lightwave Technol.* **27**, 3336-3341 (2009).
20. Gao, H., Lei, C., Chen, M., Xing, F., Chen, H. & Xie, S. A simple photonic generation of linearly chirped microwave pulse with large time-bandwidth product and high compression ratio. *Opt. Exp.* **21**, 23107-23115 (2013).
21. Zhang, H. Zou, W & Chen, J. Generation of a widely tunable linearly chirped microwave waveform based on spectral filtering and unbalanced dispersion. *Opt. Lett.* **40**, 1085-1088 (2015).
22. Li, Y., Rashidinejad, A., Wun, J. M., Leaird, D. E., Shi, J. W. & Weiner A. M. Photonic generation of W-band arbitrary waveforms with high time-bandwidth products enabling 3.9 mm range resolution. *Optica* **1**, 446-454 (2014).
23. Ghelfi, P., Laghezza, F. *et al.* A fully photonics-based coherent radar system. *Nature* **507**, 341-345 (2014).
24. McKinney, J. Technology: Photonics illuminates the future of radar. *Nature* **507**, 310-312 (2014).
25. Coppinger, F., Bhushan, A. S. & Jalali, B. Photonic time stretch and its application to analog-to-digital conversion. *IEEE Trans. Microwave Theory Tech.* **47**, 1309-1314 (1999).
26. Han, Y. & Jalali, B. Photonic time-stretched analog-to-digital converter: fundamental concepts and practical considerations. *J. Lightwave Technol.* **21**, 3085-3103 (2003).
27. Gupta, S. and Jalali, B. Time stretch enhanced recording oscilloscope. *Appl. Phys. Lett.* **94**, 041105 (2009).
28. Nuruzzaman, A., Boyraz, O. & Jalali, B. Time-stretched short-time Fourier transform. *IEEE Trans. Instrum. Meas.* **55**, 598-602 (2006).
29. Goda, K. & Jalali, B. Dispersive Fourier transformation for fast continuous single-shot measurements. *Nature Photon.* **7**, 102-112 (2013).
30. Solli, D., Chou, J. & Jalali, B. Amplified wavelength-time transformation for real-time spectroscopy. *Nature Photon.* **2**, 48-51 (2008).
31. Goda, K., Tsia, K. K. & Jalali, B. Serial time-encoded amplified imaging for real-time observation of fast dynamic phenomena. *Nature* **458**, 1145-1149 (2009).
32. Jalali, B., Chan, J. & Asghari M. H., Time-bandwidth engineering. *Optica* **1**, 23-31 (2014).
33. Jalali, B. & Mahjoubfar, A. Tailoring wideband signals with a photonic hardware accelerator. *Proceedings of the IEEE* **103**, 1071-1086 (2015).

Acknowledgements

This work was supported in part by the National Natural Science Foundation of China under Grants 61127016 and 61007052, by SRFDP of MOE (Grant No. 20130073130005), and by the State Key Lab Project of Shanghai Jiao Tong University under Grant GKZD030033. The authors are grateful to Agilent Technologies Ltd. (now Keysight Technologies Ltd.) for lending high-speed real-time oscilloscope.

Author Contributions

W.Z. and J.C. coordinated all the activities of the project. W.Z., H.Z., and J.C. designed the entire architecture, conducted the experiments, and wrote the paper. X. L. developed the data processing. S. Z. and Y. C. implemented the RF front and designed the targets.

Author Information

Correspondence and requests for materials should be addressed to Weiwen Zou (wzou@sjtu.edu.cn) or Jianping Chen (jpchen62@sjtu.edu.cn).

Additional information

The authors declare no competing financial interests.